J. Appl. Cryst. (1989). **22**, 64-69

A High-Resolution Multiple-Crystal Multiple-Reflection Diffractometer

BY PAUL F. FEWSTER

Philips Research Laboratories, Cross Oak Lane, Redhill, Surrey RH1 5HA, England

(*Received* 11 *May* 1988; *accepted* 23 *September* 1988)

Abstract

A high-resolution multiple-reflection diffractometer has been built to study crystals distorted by epitaxy and defects in nearly perfect crystals. The diffractometer combines the merits of the two-crystal four-reflection monochromator (to define a narrow wavelength range with a tailless reflectivity profile) and an analyser crystal to select the angular range diffracted from the sample crystal. The diffractometer is operated in two modes. In the first the sample and analyser rotations are coupled to obtain near-perfect rocking curves from distorted crystals, and in the second mode the two axes are uncoupled to obtain a diffraction space map for studying the diffuse scattering. The simulation of these profiles and maps based on dynamical theory is presented. The former allows complex structures to be analysed and the latter case, by deconvolving the dynamical scattering in these maps, permits a complete interpretation of the kinematic scattering.

Introduction

A four-crystal six-reflection diffractometer has been built which combines the advantages of the two-crystal four-reflection monochromator and an analyser crystal (Fig. 1). This has also been modified with a triple-reflection analyser crystal to form a four-crystal eight-reflection diffractometer. Although the experimental results presented here are for the former, the theory and applications are identical. The study of nearly perfect crystals by X-ray diffraction has in the main been undertaken by double-crystal techniques in the (+, −) configuration (Compton & Allison, 1935). The double-crystal method gives only relative lattice parameters, for example surface-layer mismatch compared with a substrate, but modifications have been made to obtain lattice parameters on an absolute scale (Hart & Lloyd, 1975; Fewster, 1982). The double-crystal method does have its limitations, in that if the Bragg angles for the first and second crystals (the latter in general being the sample) differ significantly then the diffraction profiles are broadened by the spread of wavelengths with crystal rotation angle,

$$\mathrm{d}\omega/\mathrm{d}\lambda = (\tan\theta_1 - \tan\theta_2)/\lambda. \qquad (1)$$

This can be a problem without a set of reference crystals to cover the sample materials and reflections of interest, although the realignment of the diffractometer can be relatively quick (Fewster, 1985).

The intrinsic diffraction profile from the first crystal can be very narrow and the final observed profile will be the convolution of this and the second crystal diffraction profile (James, 1962). This final diffraction profile can also be very narrow, but if the sample crystal is bent then it will diffract over an angle given by that expected convoluted with a shape function. This shape function is given by the intensity over the wavelength distribution $\Delta\lambda$,

$$\Delta\lambda = \lambda(\cot\theta)\xi, \qquad (2)$$

where ξ = (length sampled in the diffraction plane)/(radius of curvature), neglecting vertical divergence effects. The detrimental influence of bend can be partially overcome by inserting a slit between the two crystals, which reduces the sampled length in the diffraction plane, or by placing a slit in front of the detector (applicable to ω-2ω scans), thus eliminating beams outside a broad region along ω-2ω in diffraction space. However, a slit in front of the detector can accept beams of different angles from different regions of the sample.

The problem associated with the wavelength dispersion is solved by using the combined merits of the (+, −) nondispersive and (+, +) dispersive geometries, with a monochromator first proposed by DuMond (1937) for profile narrowing calculations and by Beaumont & Hart (1974) for wavelength selection and Bartels (1983) for high-resolution diffraction studies. This two-crystal four-reflection monochromator uses two *U*-shaped crystals each having its own $(n, -n)$ double-reflection geometry. The first *U*-shaped crystal produces a beam with a large wavelength spread, but each wavelength is collimated within an angular spread given by the crystal reflection. The second *U*-shaped crystal is mounted such that this beam is returned to the incident beam line from the source (Fig. 1). The third crystal reflection is set in the dispersive geometry in relation to the second reflection. But the angular acceptance of this third reflection is only the intrinsic diffraction width and therefore the wavelength can be selected and its spread determined by this width. The fourth crystal

0021-8898/89/010064-06$03.00

reflection returns the beam to its original direction with no further selection. The emergent beam from this monochromator therefore has an angular and wavelength spread determined by the intrinsic width of the crystal reflection. Since the intrinsic diffraction width of many semiconductor crystals is a few seconds of arc this can be a very useful probing beam in high-resolution diffraction (Bartels, 1983). Conditioning the beam does have its drawbacks, in that there is a significant loss in intensity, although the emergent beam for the angular range selected is only reduced at each reflection by the profile reflectivity, which for perfect crystals can be close to 1. To prevent too large a loss in intensity we can compromise by choosing a reflection with a broader rocking curve and high reflectivity. This monochromator solves the problems associated with wavelength dispersion, such that there are no restrictions on studying any reflection, but it still does not overcome the problems associated with a bent sample.

Clearly we could reduce the sampled length or use a slit at the detector in an ω–2ω scan, but these have their limitations in that a very fine slit is required, which significantly reduces the intensity in both cases and can still accept diffracted beams from different angles from different areas of the sample. These methods are not wholly satisfactory. The simplest and most elegant approach is to use an analyser crystal (Cowley, 1987; Iida & Kohra, 1979; Lal & Verma, 1984). The introduction of an analyser crystal now makes possible a reduction in the influence of sample bending, since it selects the angular range of the diffracted beam reaching the detector, which is determined by its intrinsic diffraction width. Cowley & Ryan (1987) have made use of the attributes of an analyser crystal to undertake reflectivity and low-angle scattering measurements to study the surface of silicon which was far from flat. The analyser crystal now means that we have a small diffraction space probe and the diffractometer can be used to produce a two-dimensional map of intensity (Iida & Kohra, 1979; Ryan, Hatton, Bates, Watt, Sotomayor-Torres, Claxton & Roberts, 1987). This can be extended to three-dimensional mapping by including crystal φ rotations.

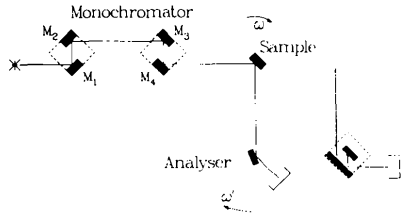

Fig. 1. The four-crystal six-reflection geometry and the alternative analyser-crystal arrangement. The sample axis of rotation, ω, and that of the detector and analyser crystal, ω', are coaxial about the front face of the sample. The three-crystal five-reflection geometry is obtained by rotating the detector to face the sample and rotating about ω' to receive the diffracted beam.

Detailed method

To understand the diffraction profiles from an instrument like this we can trace the rays through each crystal reflection.

(*a*) *Monochromator*

The profile of the beam diffracted from the first crystal face will be that for a perfect crystal, and the second crystal reflection is now just the square of this first reflection profile. The second U-shaped crystal is assumed to be perfectly set with respect to the first crystal and produces a symmetrical profile as in Fig. 2. We can see that this profile is very straight sided and has a rounded peak with negligible intensity in the tails. The full width at half maximum (FWHM) is 4·82″ arc, less than that of the intrinsic width for this reflection (5·32″ arc) and the peak intensity has been reduced to 51% reflectivity. The wavelength spread $\Delta\lambda/\lambda$ is therefore 2×10^{-5}, which is less than an order of magnitude below the FWHM of the Cu $K\alpha_1$ profile ($\Delta\lambda/\lambda = 4{\cdot}3\times10^{-4}$). The wavelength distribution over this range is therefore flat. The beam is also virtually completely polarized in the vertical plane because of the four reflections with θ close to 45°.

The profile in the horizontal plane is primarily determined by the analysis given but there is a small influence on the monochromator profile from the vertical divergence. The vertical divergence in the vertical plane $\Delta\chi$ after the first two reflections is given by

$$\Delta\chi = [2\omega(\mathrm{FWHM})/\tan\theta]^{1/2} \qquad (3)$$

where ω(FWHM) is the intrinsic FWHM for the crystal reflection. This amounts to 0·37°. Because the beam undergoes a (+, +) diffraction geometry, the accepted vertical divergence is reduced. The vertical divergence is now given by the expression $\omega(\mathrm{FWHM})/(2\Delta\chi\sin\theta_m)$, which is the ratio of the beam height acceptable to both U-shaped crystals divided by the distance to the source. θ_m is the Bragg

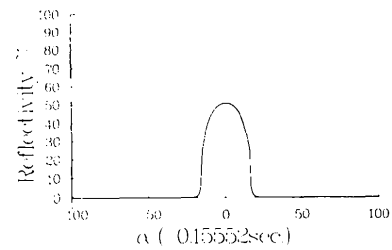

Fig. 2. The diffraction profile from the two-crystal four-reflection monochromator made from perfect Ge for the (440) planes with Cu $K\alpha$ radiation.

angle for the monochromator. This profile has a maximum angular range in the horizontal plane for this monochromator of

$$\Delta\omega_v = [\omega(\text{FWHM})/2\Delta\chi \sin\theta_m](\tan\theta\cos^2\varphi)/2. \quad (4)$$

This gives a vertical divergence angle of 0·15° for the experimental arrangement discussed and a possible profile broadening function of 0·46″ arc from a GaAs sample crystal with 004 symmetric reflection ($\varphi = 0$) and Cu Ka_1. This would be convoluted with the diffracted profile and hence have an insignificant influence on the profile.

(*b*) *Sample*

The diffraction profile obtained if the sample is rotated will be the convolution of its perfect-crystal diffraction profile with the profile given in Fig. 2. Of course, if the sample is bent then we need to convolute this profile with a further function. This shape function will be relatively flat in terms of wavelength distribution, as we have established in the last section, but will reflect the intensity distribution of the X-ray source which will be essentially Gaussian. This is the case for the three-crystal five-reflection diffractometer, without the analyser crystal.

(*c*) *Analyser*

The intrinsic diffraction curve for the analyser crystal is given in Fig. 3(*a*). This profile is that for a 111 symmetric reflection from a perfect Ge crystal and represents the acceptance range for any beam incident on the analyser crystal. The tails are greater than they need be and can be reduced by introducing more reflections as in a grooved crystal (Bonse & Hart, 1965). The calculated profile for a two-reflection and three-reflection grooved crystal are given in Fig. 3(*b*) for Ge 220 reflections. The significance of these tails will be more evident in two-dimensional diffraction mapping, discussed later. To determine the influence on the final profile from this analyser crystal we must consider the method of data collection.

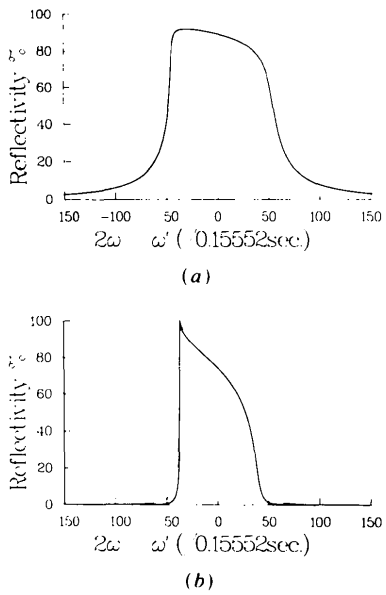

Fig. 3. The analyser reflectivity profile for Cu $K\alpha$ radiation for (*a*) a perfect Ge symmetric 111 reflection and (*b*) for a twice (dotted) and three times (line) reflected symmetric 220 grooved crystal.

ω-2ω profile scan. In this mode the sample and analyser crystals are coupled such that the analyser crystal is rotated at twice the rate of the sample crystal. The final profile will be given by

$$R(\omega) = \int_{\omega'}\int_{\alpha} R_m(\alpha)R_s(\omega-\alpha)R_a(2\omega-\omega')\,d\alpha\,d\omega'. \quad (5)$$

$R_m(\alpha)$ is the reflectivity profile for the monochromator. Clearly it is quite critical to align the maxima of the $R_s(\omega)$ sample profile and the analyser profile, R_a, such that $\omega' = 2\omega$.

ω-ω′ diffraction mapping. This mode produces additional information over that of the above, and emphasizes the power of the analyser crystal for diffraction studies. The sample and analyser crystals are uncoupled and the profile is given by

$$R_{\omega'}(\omega) = \int_{\alpha} R_s(\alpha)R_s(\omega-\alpha)R_a(2\omega-\omega')\,d\alpha \quad (6)$$

for scanning in ω for a constant analyser crystal position ω'. If we scan in ω' and fix the sample at a given position then

$$R_{\omega}(\omega') = \int_{\omega} R_m(\alpha)R_s(\omega)R_a(2\omega-\omega')\,d\omega \quad (7)$$

where $\alpha = 0$ is the centre of the monochromator distribution (*i.e.* aligned). In this way a two-dimensional map in diffraction space can be obtained and calculated. Clearly the ω'-2ω profile is contained in this map. Should the alignment ($\omega' = 2\omega$) prove difficult or the probe size be smaller than the diffraction width of the sample then this time-consuming approach might well be necessary.

The influence of a bent crystal

It was established earlier that a bent sample will result in a diffraction profile determined by the intrinsic profile convoluted with a shape function. Therefore

$$R_s(\omega) \rightarrow \int_{\beta} R_s(\omega)R_b(\beta-\omega)\,d\beta, \quad (8)$$

where $R_b(\beta)$ is the bend shape function, which, although it broadens the R_s profile, will do so only at constant ω'. Consider (5) for the ω-2ω profile scan and consider that this shape function is now modified by the analyser crystal for this scan such that it becomes $R_b(\beta)R_a(2\beta)$. Then the final diffraction

profile is given by

$$R(\omega) = \int_{\beta} \left[\int_{\alpha} R_m(\alpha) R_s(\omega - \alpha)\, \mathrm{d}\alpha \right] \times R_b(\beta - \omega) R_a(2\beta - 2\omega)\, \mathrm{d}\beta \qquad (9)$$

and it is clear that the influence of a bent sample is restricted by the analyser profile function. Since the sample is rotated at half the step size of the analyser crystal the maximum FWHM is half the intrinsic FWHM for the analyser crystal. The alignment of the peak reflectivity of the analyser and the sample is less critical if the sample is bent, since we would be trying to match the peak reflectivity for R_a and $R_s * R_b$, where $*$ represents a convolution.

The influence of bending on the two-dimensional map can be observed from (6) and (7), which can be rewritten as

$$R_{\omega'}(\omega) = \int_{\beta} \left[\int_{\alpha} R_m(\alpha) R_s(\omega - \alpha) R_a(2\omega - \omega')\, \mathrm{d}\alpha \right] \times R_b(\beta - \omega)\, \mathrm{d}\beta \qquad (10)$$

and

$$R_{\omega}(\omega') = \int_{\omega} R_m(\alpha) R_s(\omega) R_a(2\omega - \omega')\, \mathrm{d}\omega. \qquad (11)$$

Clearly the profile along ω is broadened by the convolution with R_b along the direction of constant ω', whereas in the ω' direction there is no influence since the broadening function introduced here is assumed to bend the crystallographic planes and not to distort the lattice (*i.e.* there are no strain effects which would have a 2θ component), but it is broadened by the convolution of the analyser profile R_a.

On considering the three-crystal five-reflection diffractometer (without the analyser crystal) we see that the detector window will have a flat response (barring imperfections in the window) and (10) will reduce to

$$R(\omega) = \int_{\beta} \left[\int_{\alpha} R_m(\alpha) R_s(\omega - \alpha)\, \mathrm{d}\alpha \right] R_b(\beta - \omega)\, \mathrm{d}\beta \qquad (12)$$

and is equivalent to (9) where $R_a(2\omega - \omega')$ is single-valued and unity. From this it is clear that the bend has a significant influence on the profile. The use of a slit will give a more rectangular function for $R_b(\beta)$ but, as mentioned previously, this is not truly angularly selective.

Experimental

The four-crystal six-reflection diffractometer was built by modifying an Apex goniometer (Baker, George, Bellamy & Causer, 1966). The monochromator, composed of two *U*-shaped germanium crystals with (110) faces, replaced the original collimator and is comparable in length. The analyser crystal is a perfect germanium crystal set to the 111 symmetric reflection and was mounted on the 2θ arm with the detector offset. The sample was mounted in an identical manner to that described by Fewster (1985) and aligned in the same way. An example of the two modes of the diffractometer will be given to illustrate the advantages of this geometry over the three-crystal five-reflection method.

ω–2ω mode

The sample studied is shown schematically in Fig. 4, and the high-resolution rocking curve without the analyser crystal is given in Fig. 5. The sample is clearly bent and this rocking curve yields little information. The four-crystal six-reflection rocking curve is also displayed. Experimentally this is obtained by rotating the 2θ arm of the diffractometer for the analyser crystal to receive the diffracted beam. It is clear that the rocking curve is very different and much more information can be gleaned. The peak intensity has dropped by only 30% and the signal-to-noise ratio is improved by an order of magnitude. With additional information on the structural period obtained on a

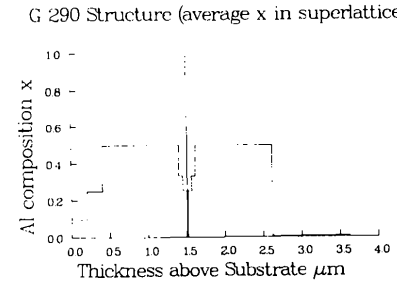

Fig. 4. The average composition profile through an all-binary superlattice $Al_xGa_{1-x}As$-based laser structure. The average composition x at any point in the structure was obtained by growing a few monolayers of AlAs and GaAs in the correct proportions by molecular beam epitaxy. The structure was composed of 1517 layers.

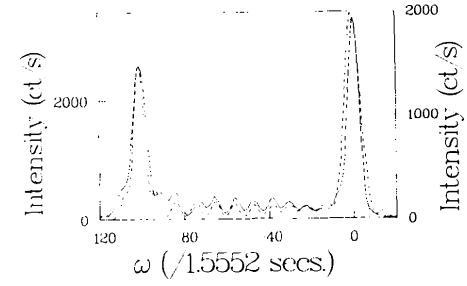

Fig. 5. The rocking curve obtained with Cu $K\alpha$ for G290 with the three-crystal five-reflection geometry (dotted) and the four-crystal six-reflection geometry (line). The best-fit computer-simulated profile from Fig. 6 calculated for the four-crystal six-reflection geometry with equation (9) is also given (dashed).

powder diffractometer (Fewster, 1987) the 004 high-resolution profile $R_s(\omega)$ could be modelled using dynamical theory in the manner given by Fewster & Curling (1987) and computer-assisted fitting (unpublished work). We can predict the bend shape profile $R_b(\beta)$ for comparing this fitted profile (Fig. 6) with that from the three-crystal five-reflection diffractometer. The simulated profile for the four-crystal six-reflection geometry is given in Fig. 5, calculated from (9) on the basis of the best fit profile from the four-crystal six-reflection diffractometer $R_s(\omega)$ (Fig. 6), the predicted bend shape profile $R_\beta(\omega)$ and the known profiles $R_m(\alpha)$ and $R_a(\omega')$. Note that the detailed fringing on a substrate peak (Fig. 6) is not observed experimentally; this would require an even finer probe (*i.e.* with even narrower monochromator and analyser profiles). The required structural details, *viz* composition as a function of depth, could be obtained for this structure, which would not have been possible using a conventional diffractometer.

ω–ω' mapping

The experimental map around the 004 diffraction point is given in Fig. 7 for the sample G259 (consisting of 60 periods of 28 Å GaAs + 75 Å AlAs capped with 0·1 μm GaAs, all on a GaAs substrate). The three-crystal five-reflection geometry was used initially to obtain a standard diffraction profile and the best-fit model was simulated to give the profile $R_s(\omega)$ and the shape function $R_b(\beta)$ (Fig. 8). The map was then simulated with $R_s(\omega)$, $R_b(\beta)$ and the known profiles $R_m(\alpha)$ and $R_a(\omega')$. This simulated diffraction map is given in Fig. 9 and is a reasonably good fit to the experimental map (Fig. 7). We could at this stage compare the experimental and calculated maps to yield any unexplained features, *e.g.* the structural features leading to this diffuse scattering that make each peak more rounded or elongated in the $q_\parallel$ direction than can be explained by assuming the crystal to be absolutely perfect. The rounding of the peaks is likely to arise from local defects, giving a 3D diffuse scattering distribution from a spherical strain field. The elongation in the $q_\parallel$ direction could well arise from the mosaic nature of the material, *i.e.* local

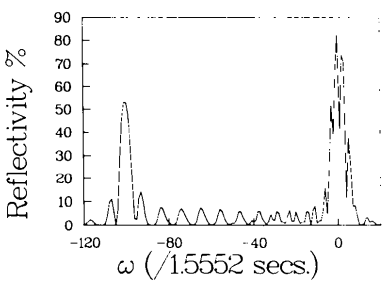

Fig. 6. The perfect-crystal rocking curve for G290 simulated from the parameters derived from the four-crystal six-reflection rocking curve of Fig. 5.

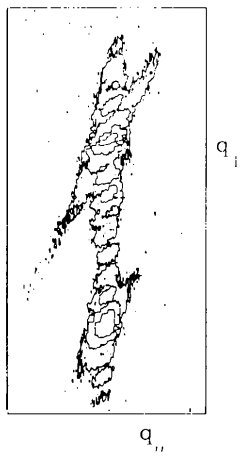

Fig. 7. The diffraction map obtained from sample G259 (drawn in reciprocal-space coordinates) around the 004 reflection (Cu $K\alpha$) contoured on a logarithmic scale commencing at 1 count s^{-1} with 0·5 count s^{-1} background intensity removed. The high region of intensity at the top of the figure comes predominately from the substrate and that at the bottom comes predominately from the multiple-quantum-well layer. The total $q_\perp$ and $q_\perp$ ranges plotted are 0·01 and 0·02 $Å^{-1}$ respectively, where $q_\perp$ is parallel to [001] (perpendicular to the sample surface) and $q_\parallel$ is parallel to [110] (parallel to the sample surface).

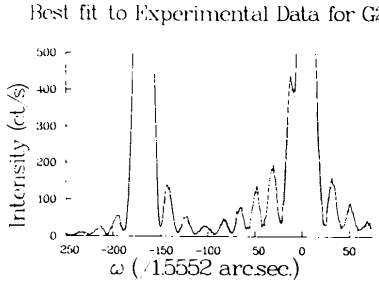

Fig. 8. The experimental five-crystal reflection rocking curve for the 004 reflection (Cu $K\alpha$) for G259 and the best-fit profile for deriving R_s and R_b.

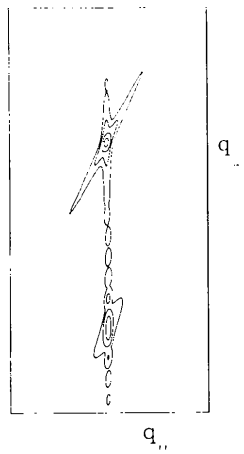

Fig. 9. The simulated diffraction map of Fig. 7, where the peak intensities are equated and the contours compare directly with those in Fig. 7.

misorientations (their misorientation will determine the breadth of the profile), and will be independent of any strain component. The interpretation will be covered in a future publication.

The long tails in the diffraction maps can be eliminated by using a multiple-reflection analyser crystal. The acceptance profile given in Fig. 3(*b*) for a three-reflection analyser was used to calculate the diffraction map for sample G259 and is given in Fig. 10. This is clearly an improvement with the loss of little intensity, although the rapidly varying profile (Fig. 3*b*) can lead to problems when operating the diffractometer in the ω-2ω mode compared with using the very flat 111 profile (Fig. 3*a*), since matching the condition $\omega' = 2\omega$ is considerably more difficult (requiring very stable conditions). The monochromator could also be used in the lower-resolution mode to enhance the intensity (220 reflections, where the FWHM for the emergent beam is 11·8″ of arc and a similar shaped profile to that in Fig. 2). A further improvement would be the addition of a high-power source to replace the conventional sealed-tube source used in these experiments to enhance the weak diffuse scattering.

Concluding remarks

This diffractometer has opened new possibilities for analysing complex multilayer structures bent through epitaxial growth or distorted for some other reason. The benefits of the two-crystal four-reflection monochromator also allow investigation of any crystal reflections without the effects of wavelength dispersion. This diffractometer has proved very successful for investigating semiconductor structures and is very simple and quick to set up and achieve results. It is especially valuable for grazing-incidence studies which rely heavily on overcoming the influence of bend in the samples and it also removes the necessity for complex slit arrangements in the diffracted beam.

The ability to measure and calculate diffraction maps to high resolution around reciprocal-lattice points, for studying diffuse scattering and peak shapes, will yield structural information not observed by diffractometers without any analyser crystal. The influence of strain broadening and misorientated regions of the crystal or defects can be resolved with this diffractometer. The simulation of these diffraction maps permits the dynamical scattering component to be deconvoluted to leave the kinematically scattered intensity, which is amenable for determining defect sizes and distributions.

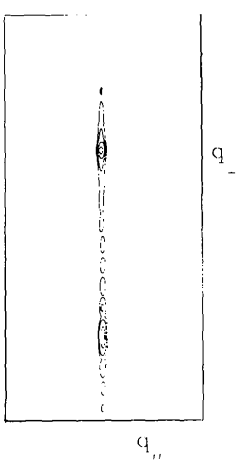

Fig. 10. A similar simulated map as Fig. 9, with the same contour levels, but obtained with the alternative analyser [three times reflected (Fig. 3*b*)].

I am indebted to Dr J. A. Morice for his help in the programming aspects of generating the data for the simulated maps and Mr R. S. Cole for programming the contouring and plotting routines for these two-dimensional diffraction maps. I would also like to acknowledge Dr C. T. B. Foxon for the MBE growth of the structures given as examples of the diffractometer's capabilities.

References

BAKER, T. W., GEORGE, J. D., BELLAMY, B. A. & CAUSER, R. (1966). *Nature (London)*, **210**, 720-721.
BARTELS, W. J. (1983). *J. Vac. Sci. Technol. B*, **1**, 338-345.
BEAUMONT, J. H. & HART, M. (1974). *J. Phys. E*, **7**, 823-839.
BONSE, U. & HART, M. (1965). *Appl. Phys. Lett.* **7**, 238-240.
COMPTON, A. H. & ALLISON, S. K. (1935). *X-rays in Theory and Experiment*, pp. 709-740. New York: Van Nostrand.
COWLEY, R. A. (1987). *Acta Cryst.* A**43**, 825-836.
COWLEY, R. A. & RYAN, T. W. (1987). *J. Phys. D*, **20**, 61-68.
DUMOND, J. W. M. (1937). *Phys. Rev.* **52**, 872-883.
FEWSTER, P. F. (1982). *J. Appl. Cryst.* **15**, 275-278.
FEWSTER, P. F. (1985). *J. Appl. Cryst.* **18**, 334-338.
FEWSTER, P. F. (1987). *Thin-Film Growth Techniques for Low-Dimensional Structures. NATO ASI Series B: Physics*, Vol. 163, edited by R. F. C. FARROW, S. S. P. PARKIN, P. J. DOBSON, J. H. NEAVE & A. S. ARROTT, pp. 417-440. New York: Plenum Press.
FEWSTER, P. F. & CURLING, C. J. (1987). *J. Appl. Phys.* **62**, 4154-4158.
HART, M. & LLOYD, K. H. (1975). *J. Appl. Cryst.* **8**, 42-44.
IIDA, A. & KOHRA, K. (1979). *Phys. Status Solidi A*, **51**, 533-542.
JAMES, R. W. (1962). *The Optical Principles of the Diffraction of X-rays*, pp. 306-318. London: Bell.
LAL, K. & VERMA, A. R. (1984). *Bull. Mater. Sci.* **6**, 129-149.
RYAN, T. W., HATTON, P. D., BATES, S., WATT, M., SOTOMAYOR-TORRES, S., CLAXTON, P. A. & ROBERTS, J. S. (1987). *Semicond. Sci. Technol.* **2**, 241-243.